

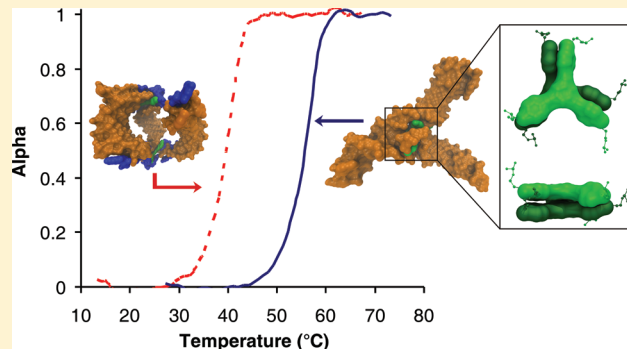
# Enhancing the Melting Properties of Small Molecule-DNA Hybrids through Designed Hydrophobic Interactions: An Experimental-Computational Study

Ibrahim Eryazici, Ilyas Yildirim, George C. Schatz,\* and SonBinh T. Nguyen\*

Department of Chemistry, Northwestern University, 2145 Sheridan Road, Evanston, Illinois 60208, United States

## Supporting Information

**ABSTRACT:** Detailed experimental and computational studies revealed the important role that hydrophobic interactions play in the aqueous assembly of rigid small molecule-DNA hybrid (rSMDH) building blocks into nanoscale cage and face-to-face (ff) dimeric structures. In aqueous environments, the hydrophobic surfaces of the organic cores in these nanostructures are minimized by interactions with the core in another rSMDHs, with the bases in the attached DNA strands, and/or with the base pairs in the final assembled structures. In the case that the hydrophobic surfaces of the cores could not be properly isolated in the assembly process, an ill-defined network results instead of dimers, even at low concentration of DNA. In contrast, if ff dimers can be formed with good minimization of the exposed hydrophobic surfaces of the cores, they are highly stable structures with enhanced melting temperatures and cooperative melting behavior.



## INTRODUCTION

Among natural biopolymers, DNA and RNA possess the unique ability to self-assemble into a unique double-stranded helix form in ionic media, based on a combination of H-bonding of bases,  $\pi-\pi$  stacking of base pairs, and electrostatic stabilization of the phosphate backbone.<sup>1</sup> The stable DNA-based helix, with a diameter of  $\sim 2$  nm and persistence length of  $\sim 50$  nm, has long been used as the sole building block for engineering 2D<sup>2–5</sup> and 3D<sup>6–9</sup> nanostructures that are used to pattern nanoparticles<sup>10,11</sup> and biomolecules<sup>12–14</sup> on solid surfaces for electronic and biosensor applications. DNA has also been linked to rigid<sup>15–24</sup> and flexible (dendritic<sup>25–27</sup>) organic molecules, polymers,<sup>28–30</sup> metal complexes,<sup>31–37</sup> and nanoparticles<sup>38,39</sup> to be used for highly selective DNA detection<sup>40–42</sup> and to direct the assembly of those particles<sup>43–47</sup> and complexes<sup>48,49</sup> in a predesigned fashion for electronic applications.

The assembly of organic-DNA hybrids into nanostructures in aqueous media has generally been explored using three basic parameter groups: (1) the number of single strand (ss) DNA chains that are attached to the organic “core” fragment; (2) the orientation, geometry, and concentration of these strands; and (3) the type ( $\text{Na}^+$ ,  $\text{K}^+$ ,  $\text{Ca}^{2+}$ ,  $\text{Mg}^{2+}$ , etc.) and concentration of salts. Surprisingly, the role of the organic core in the assembly of nanoscale organic-DNA structures has rarely been investigated even though the core fragment can often be quite hydrophobic and should have significant interactions with the bases/base pairs in ionic media. Indeed, the hydrophobic interaction of rigid organic groups such as stilbenes and

anthraquinones with DNA bases or base pairs has been utilized to stabilize small duplex DNA-detection probes to improve their target affinity and specificity.<sup>50,51</sup> In a related report, small DNA hairpins have been shown to exhibit enhanced stability when they are end-capped with rigid organic molecules.<sup>52</sup> Given these precedents, it is surprising that only a few studies to date have examined the roles that hydrophobic interactions play in the assembly of organic-DNA building blocks into larger structures. Notably, perylene diimide (PDI)-DNA hybrids have been found to form both hairpin dimers<sup>53</sup> based on double-helix DNA assembly as well as larger supramolecular oligomers involving hydrophobic interactions of the PDI cores with each other via hydrophobic stacking.<sup>16,18</sup>

Herein, we present a comprehensive experimental and computational study to understand the roles that rigid, hydrophobic organic cores play in the assembly of rigid small molecule-DNA hybrids (rSMDHs), which are molecules composed of several ss-DNAs attached to a rigid organic core, into discrete nanostructures (Figure 1). We found the final nanostructures to have been assembled in aqueous environments in a way that minimizes the exposure of the hydrophobic surface of the organic core in rSMDH, through interactions with the core in another rSMDH, with the bases in the attached DNA strands, and/or with the base pairs in the final assembled structures. To evaluate the importance of these hydrophobic interactions, we prepared two distinct dimer

Received: January 12, 2012

Published: March 19, 2012

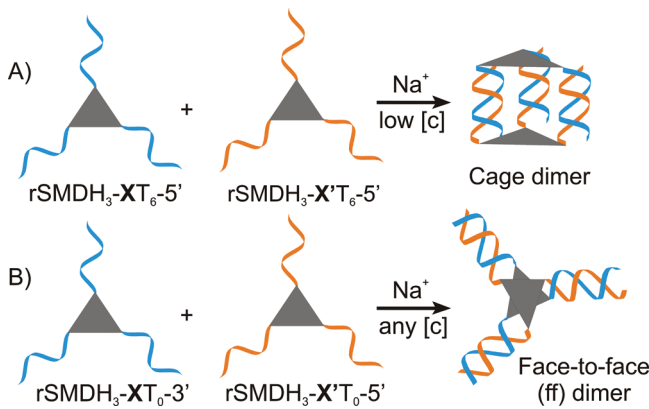


**Figure 1.** A schematic representation of the assembly of rSMDH<sub>3</sub>-XT<sub>6</sub>-5' and its complementary rSMDH<sub>3</sub>-X'T<sub>6</sub>-5' into a cage dimer (A) and the assembly of rSMDH<sub>3</sub>-XT<sub>0</sub>-3' and its complementary rSMDH<sub>3</sub>-X'T<sub>0</sub>-5' into a ff dimer (B). Gray triangle depicts an organic core; [c] denotes the total concentration of the ss-DNA arms.

assemblies (cage and face-to-face (ff)) from complementary rSMDH<sub>3</sub>'s where the solvent-accessible surface area (SASA) of the hydrophobic cores can be tuned by polythymine spacers or by controlling the orientation of the three attached ss-DNA strands (Figure 1). Compared to the cage dimer (Figure 1A), which melts (i.e., dehybridizes) at 3 °C higher than its DNA duplex components, the ff assembly (Figure 1B) showed a dramatic enhancement in melting properties (by 15 °C) due to interaction of the two rigid, hydrophobic cores with each other and their “intercalation” into the DNA assembly, as explained by molecular dynamics (MD) simulations. These results strongly suggest that hydrophobic interactions can significantly affect the structures and properties of nanostructures constructed from organic-DNA hybrids. Thus, hydrophobic interactions should be considered as a major parameter in the design of nanoscale assemblies from organic-DNA (or polymer-DNA) building blocks, together with the number of ss-DNA surrounding the organic core; the orientation, geometry and concentration of the strands; and the type and concentration of the salts in the assembly media.

## RESULTS AND DISCUSSIONS

**Synthesis of rSMDH<sub>3</sub> Building Blocks.** We previously reported the formation of cage dimers (Figure 1A) based on the hybridization of two rigid small molecule-DNA hybrids

containing three DNA arms (rSMDH<sub>3</sub>), each comprising 15-bp complementary and 6-bp (T<sub>6</sub>) non-complementary bases, at low concentrations.<sup>21</sup> Similar cage assemblies comprising DNA-hybrids have also been mentioned by the von Kiedrowski,<sup>26</sup> Southern,<sup>27</sup> and Sawai groups.<sup>19</sup> The theses of these previous papers were primarily focused on the assembly and characterization of these cage assemblies as well as their melting properties; the effects of the cores and non-complementary spacers in the assembly process were very much ignored. In light of recent reports on the important roles that hydrophobic interactions and steric constraints may play in the assembly of DNA-linked nanostructures,<sup>16,18</sup> we became interested in elucidating the effects of non-complementary T<sub>n</sub> (*n* = 0, 3, and 6) spacers upon the assembly and stability of cage dimers possessing large hydrophobic organic cores. As part of this effort, we improved the stability of the linkage of our organic core (C) to DNA by adding an extra glycolic moiety (−CH<sub>2</sub>CH<sub>2</sub>O−) to all the termini (see core C in Figure 2) of our original 1,3,5-tris(*p*-ethynylphenyl)benzene organic core.<sup>23</sup> We also improved the earlier core synthesis to make it more conducive to scale-up and purification (see Scheme S1 in the Supporting Information for the synthesis of core C).

The synthesis of symmetric rSMDH<sub>3</sub> was achieved in good yields in two steps: the phosphoramidite core C is first attached to either the 3' or 5' end of single-strand oligonucleotides (15-to-21-base pair (bp)) grown from the surface of controlled porosity glass beads (CPG). The second and third arms are then simultaneously grown from the resulting core C-functionalized CPG via 3'-normal or 5'-reverse phosphoramidite chemistry (Figure 2). The final DMT-protected products were then cleaved from the solid support and purified by reverse-phase HPLC, and then DMT is deprotected to yield the desired rSMDH<sub>3</sub>'s. This synthesis afforded a library of rSMDH<sub>3</sub>'s, in which three of the same single-strand oligonucleotides (15 complementary and 0–6 (T<sub>0</sub>, T<sub>3</sub>, and T<sub>6</sub>) non-complementary bases) are connected to the rigid core C from either the 3' or 5' end (Table 1, entry 1–9). The purity of all rSMDH<sub>3</sub>'s was ascertained via analytical reverse-phase HPLC and their length and base compositions were confirmed via MALDI-ToF mass spectrometry (see Supporting Information for more details).

**Self-Assembly of Cage Dimers.** Combining equimolar amounts of rSMDH<sub>3</sub>-XT<sub>n</sub>-5' (*n* = 0, 3, and 6) and its complement rSMDH<sub>3</sub>-X'T<sub>n</sub>-5' (*n* = 0, 3, and 6) (or rSMDH<sub>3</sub>-YT<sub>3</sub>-3' and its complement rSMDH<sub>3</sub>-Y'T<sub>n</sub>-3') at low concen-

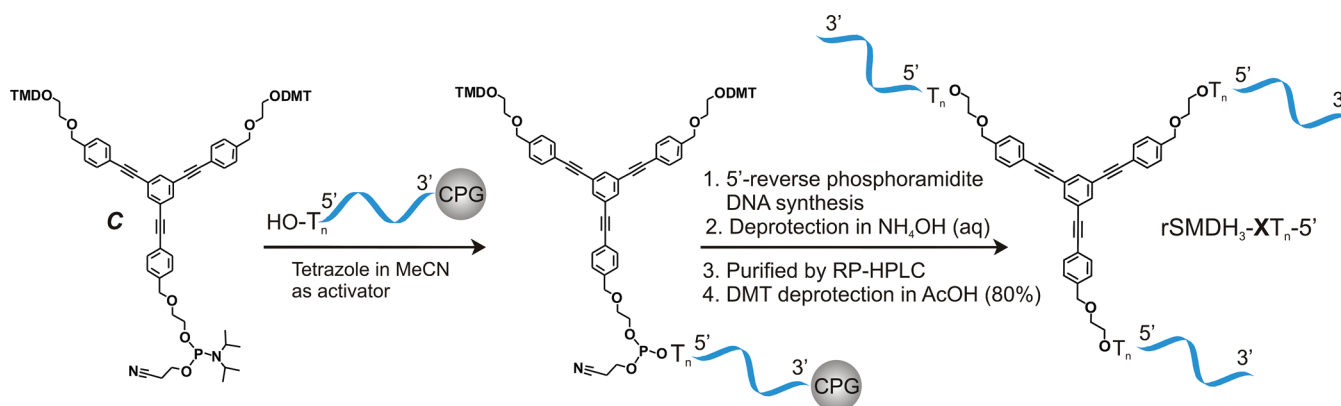


**Figure 2.** Schematic presentation of the synthesis of rSMDH<sub>3</sub>-XT<sub>n</sub>-5' (Table 1, *n* = 0, 3, and 6) using 3'- and 5'-phosphoramidite chemistry. Other sequences listed in Table 1 were synthesized using the same synthetic methodology.

**Table 1.** Single-strand rSMDH<sub>3</sub> Oligonucleotides Used in This Work

entry	short name	orientation
1	rSMDH <sub>3</sub> -XT <sub>0</sub> -5'	(3'-X-5') <sub>3</sub> C
2	rSMDH <sub>3</sub> -XT <sub>3</sub> -5'	(3'-X-T <sub>3</sub> -5') <sub>3</sub> C
3	rSMDH <sub>3</sub> -XT <sub>6</sub> -5'	(3'-X-T <sub>6</sub> -5') <sub>3</sub> C
4	rSMDH <sub>3</sub> -XT <sub>0</sub> -5'	(3'-X'-5') <sub>3</sub> C
5	rSMDH <sub>3</sub> -XT <sub>3</sub> -5'	(3'-X'-T <sub>3</sub> -5') <sub>3</sub> C
6	rSMDH <sub>3</sub> -XT <sub>6</sub> -5'	(3'-X'-T <sub>6</sub> -5') <sub>3</sub> C
7	rSMDH <sub>3</sub> -XT <sub>0</sub> -3'	(5'-X-3') <sub>3</sub> C
8	rSMDH <sub>3</sub> -YT <sub>3</sub> -3'	(5'-Y-T <sub>3</sub> -3') <sub>3</sub> C
9	rSMDH <sub>3</sub> -YT <sub>3</sub> -3'	(5'-Y-T <sub>3</sub> -3') <sub>3</sub> C

sequence X: 3'-ATC CTT ATC AAT ATT-5'  
sequence X': 5'-TAG GAA TAG TTA TAA-3'  
sequence Y: 3'-TTA TAA CTA TTC CTA-5'  
sequence Y': 5'-AAT ATT GAT AAG GAT-3'

trations (2  $\mu$ M total ss-DNA concentration, in which each arm's concentration in the rSMDH<sub>3</sub> was calculated separately) were expected to result in cage structures (Figure 1A, listed in Table 2) as previously reported.<sup>19,21,26,27</sup> A low-concentration

**Table 2.** Double-strand rSMDH<sub>3</sub> Assemblies, Including Cage Dimers and Their Controls, Used in This Work

entry	components <sup>a</sup>	short name
1	rSMDH <sub>3</sub> -XT <sub>0</sub> -5':rSMDH <sub>3</sub> -XT <sub>0</sub> -5'	cage-T <sub>0</sub> -T <sub>0</sub> <sup>b</sup>
2	rSMDH <sub>3</sub> -XT <sub>3</sub> -5':rSMDH <sub>3</sub> -XT <sub>3</sub> -5'	cage-T <sub>3</sub> -T <sub>3</sub>
3	rSMDH <sub>3</sub> -XT <sub>6</sub> -5':rSMDH <sub>3</sub> -XT <sub>6</sub> -5'	cage-T <sub>6</sub> -T <sub>6</sub>
4	rSMDH <sub>3</sub> -YT <sub>3</sub> -3':rSMDH <sub>3</sub> -YT <sub>3</sub> -3'	cage-T <sub>3</sub> -T <sub>3</sub> -reverse
5	rSMDH <sub>3</sub> -XT <sub>0</sub> -5':3X	control-rSMDH <sub>3</sub> -T <sub>0</sub>
6	rSMDH <sub>3</sub> -XT <sub>3</sub> -5':3X	control-rSMDH <sub>3</sub> -T <sub>3</sub>
7	rSMDH <sub>3</sub> -XT <sub>6</sub> -5':3X	control-rSMDH <sub>3</sub> -T <sub>6</sub>

<sup>a</sup>Total DNA concentration of 1 and 2  $\mu$ M. <sup>b</sup>This structure did not form according to PAGE-gel study (see Figure 3).

experimental range is required for cage dimer formation because at higher concentrations (>2  $\mu$ M total ss-DNA concentration) rSMDH<sub>3</sub>'s tend to form other ill-defined networks much larger in size than the dimer cages.<sup>20,21</sup>

Non-denaturing PAGE-gel analysis of the [rSMDH<sub>3</sub>-XT<sub>n</sub>-5':rSMDH<sub>3</sub>-XT<sub>n</sub>-5'] and [rSMDH<sub>3</sub>-YT<sub>n</sub>-5':rSMDH<sub>3</sub>-YT<sub>n</sub>-5'] combinations confirmed the formation of the expected cage T<sub>n</sub>-T<sub>n</sub> ( $n = 3$  and 6) structures (Figure 3). The three combinations that we attempted all afforded a main band (Figure 3A, lanes 5, 7, and 8) that is slightly slower in mobility compared to the corresponding [rSMDH<sub>3</sub>-XT<sub>n</sub>-5':3X] control groups (Figure 3A, lanes 2, 4, and 6), which were prepared by hybridizing 3 equiv of single-stranded 3'-X-5' with rSMDH<sub>3</sub>-XT<sub>n</sub>-5' ( $n = 0, 3$ , and 6, see Table 2, entries 5–7). In contrast, the T<sub>0</sub>-T<sub>0</sub> combinations did not form the intended cages: the [rSMDH<sub>3</sub>-XT<sub>0</sub>-5':rSMDH<sub>3</sub>-XT<sub>0</sub>-5'] combination yielded a high-molecular-weight single band that did not move in the non-denaturing PAGE-gel (Figure 3A, lane 3). Such a high-molecular-weight material has been characterized by Sleiman and co-workers using atomic force microscopy (AFM)<sup>20</sup> as being an ill-defined network comprising hundreds of rSMDH<sub>3</sub>'s and being much bigger than the 500-bp DNA ladder (Figure 3A, lane 1).

Evidence for cage formation in the [rSMDH<sub>3</sub>-XT<sub>n</sub>-5':rSMDH<sub>3</sub>-XT<sub>n</sub>-5'] and [rSMDH<sub>3</sub>-YT<sub>n</sub>-5':rSMDH<sub>3</sub>-YT<sub>n</sub>-5'] combinations is afforded by the close similarities in the

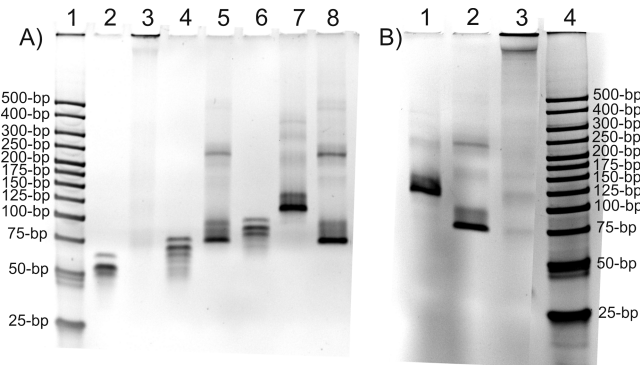


**Figure 3.** Non-denaturing PAGE-gel image (6%) of DNA assemblies with (A) 2  $\mu$ M total ss-DNA concentration. From left to right: lane 1 = HLS DNA ladder, lane 2 = control-rSMDH<sub>3</sub>-T<sub>0</sub>, lane 3 = cage-T<sub>0</sub>-T<sub>0</sub>, lane 4 = control-rSMDH<sub>3</sub>-T<sub>3</sub>, lane 5 = cage-T<sub>3</sub>-T<sub>3</sub>, lane 6 = control-rSMDH<sub>3</sub>-T<sub>6</sub>, lane 7 = cage-T<sub>6</sub>-T<sub>6</sub>, lane 8 = cage-T<sub>3</sub>-T<sub>3</sub>-reverse; (B) 1  $\mu$ M total ss-DNA concentration. From left to right: lane 1 = cage-T<sub>6</sub>-T<sub>6</sub>, lane 2 = cage-T<sub>3</sub>-T<sub>3</sub>-reverse, lane 3 = cage-T<sub>0</sub>-T<sub>0</sub>, lane 4 = HLS DNA ladder. Please refer to Table 2 for explanations of the short names.

mobilities of these combinations on non-denaturing PAGE-gel against those of the [rSMDH<sub>3</sub>-X'T<sub>n</sub>-5':3X] control groups. These latter groups provides a better reference point than commercially available linear DNA ladders (i.e., HyperLadder V) for sizes and mobilities of three-arm rSMDH<sub>3</sub>'s (Table 2) in a PAGE-gel study because the DNA arms are linked to one organic core and the overall assembly can better reflect the charge/hydrodynamic volume ratio for rSMDH<sub>3</sub>'s. We note with interest that all control assemblies, control-rSMDH<sub>3</sub>-T<sub>n</sub> ( $n = 0, 3$ , and 6; Table 2, entries 5–6), displayed several bands around a single dark spot in the gel (Figure 3A, lanes 2, 4, and 6) that can be attributed to the different conformations of the arms in the assemblies, distinguishable at 4 °C where the PAGE-gel experiment was carried out.<sup>54</sup>

We also attempted to assemble cage-T<sub>0</sub>-T<sub>0</sub> at a lower DNA concentration (1  $\mu$ M), knowing that this would favor the formation of discrete cage dimers over ill-defined network.<sup>23</sup> Nevertheless, the PAGE-gel experiment again showed exclusive formation of high-molecular-weight networks that did not move on the gel (Figure 3B). Given that the other rSMDH<sub>3</sub>'s with non-complementary T<sub>3</sub> and T<sub>6</sub> spacers can form cages (Figure 3A), we suspected that concentration is not the only factor that dictate the formation of small cages or large networks. Rather, the presence of the non-complementary thymine spacers can significantly influence the product formation. As such, we turn to MD simulations to help us elucidate the difference in assembly formation between rSMDH<sub>3</sub> with T<sub>0</sub> spacer and those with T<sub>3</sub> and T<sub>6</sub> spacers.

#### Molecular Dynamics Simulations of Cage Systems.

For small DNA duplexes that were assembled from organic-DNA hybrids, the interactions between the organic group with DNA bases and base pairs can exert a significant influence on the final properties of the assembled organic-DNA duplexes. In contrast, the influence of the organic group in the assembly process and the final properties of large DNA-hybrid structures comprising more than one DNA duplex have not been evaluated in detail by computational modeling. While computational tools such as coarse-grain simulations<sup>55,56</sup> are available, they are low-resolution and were mainly used to simulate large DNA nanostructures to study their melting, mechanical, and

conformational properties.<sup>55–58</sup> In-depth, atomistic-level computational methods have not been applied to study the assembly of DNA-hybrids into large structures (>20 nm), so-called supramolecular DNA assemblies,<sup>59</sup> due to their inability to give meaningful data for time scales that are comparable to the dynamics of biological polymers. However, MD simulations with atom-based force fields, such as AMBER<sup>60–62</sup> and CHARMM,<sup>63,64</sup> are starting to gain ground through improvements in computational technology.<sup>65</sup> Millisecond-long atomistic-level MD simulations can now be performed to shed light on the assembly mechanism of complex systems.<sup>66</sup> As such, we set out to model the assembly of the aforementioned [rSMDH<sub>3</sub>-XT<sub>n</sub>-S':rSMDH<sub>3</sub>-X'T<sub>n</sub>-S'] assemblies using MD simulation.

Model systems for cage-T<sub>n</sub>-T<sub>n</sub> ( $n = 0, 3$ , and  $6$ ) were created with the AMBER<sup>60–62</sup> simulation packages. The organic core was parametrized with the AMBER GAFF force field,<sup>67</sup> and restrained electrostatic potential (RESP) charges of the core's atoms were derived following the RESP protocol (see Supporting Information for details).<sup>68–71</sup> For DNA duplexes, amber99 force field,<sup>69,72</sup> with revised  $\chi^2$  and  $\alpha/\gamma^2$  torsional parameter sets, were used. Initial structures of the cage dimers were constructed with shortened versions of rSMDH<sub>3</sub>-XT<sub>n</sub>-S' and rSMDH<sub>3</sub>-X'T<sub>n</sub>-S', each comprising three 10-bp ds-DNA in B-form conformation that are attached to the organic cores. In the initial configuration, the cores were positioned in the model as far away as possible from DNA bases and base pairs (Figure 4A–C). For each assembly, four independent, implicit-solvent<sup>75,76</sup> MD simulations were performed and each simulation was 100 ns long. At the end of the simulations, the cores in cage-T<sub>3</sub>-T<sub>3</sub> and cage-T<sub>6</sub>-T<sub>6</sub> (Figure 3E,F) were observed to be uniformly interacting with non-complementary thymine bases. The core for cage-T<sub>0</sub>-T<sub>0</sub> was observed to intercalate into the closest base pairs, which significantly

"deform" the structure (Figure 4D). These results suggest that the cage assemblies have reorganized to minimize the hydrophobic surfaces of the cores in aqueous environments at the detriment of the caged structure.

To qualitatively estimate the hydrophobic surface area of the core that is exposed to water throughout the simulation (100 ns), we performed a SASA analysis of trimer cores in the cage assemblies using the AREAIMOL program (ver. 6.2.0) from CCP4.<sup>77</sup> With only the benzyl and acetylenes moieties of the trimer cores included as hydrophobic moieties in these calculations, the total SASA of two fully exposed cores in each cage assembly at the start of the simulations was calculated to be  $\sim 1620 \text{ \AA}^2$ . Then the final SASA data of the assemblies were calculated by averaging the last 50 ns of each set of simulations (Table S6 and Figures S41–S46 in Supporting Information). Each SASA value was mean-averaged over four set of simulations and reported with the appropriate standard deviation (Figure 4, SASA values are listed under each image). After 100 ns, the SASAs of the trimer cores were reduced from the initial  $\sim 1620 \text{ \AA}^2$  value to 469, 347, and  $252 \text{ \AA}^2$  for cage-T<sub>0</sub>-T<sub>0</sub>, cage-T<sub>3</sub>-T<sub>3</sub>, and cage-T<sub>6</sub>-T<sub>6</sub>, respectively. From the final structures (Figure 4), it is clear cage-T<sub>3</sub>-T<sub>3</sub> and cage-T<sub>6</sub>-T<sub>6</sub> assemblies are better able in reducing the initial core SASA (by 79–86%) than cage-T<sub>0</sub>-T<sub>0</sub> (by only 71%) because they have non-complementary thymine spacers that can wrap around the cores (Figure 4E,F) to reduce their SASA. This is not the case for cage T<sub>0</sub>-T<sub>0</sub>, which was forced to dehybridize the terminal base pairs so that the cores can interact with the individual bases and minimize its exposed hydrophobic surface (Figure 4D). This, however, distorts and destabilizes the DNA duplexes from their stable B-form conformation as reflected in the decreased total number of hydrogen bonds (see discussion below).

At the beginning of the simulations, the total number of H-bonds within the hybridized DNA duplex arms for all cage systems was calculated to be 69. However, 13 of these bonds were broken in cage-T<sub>0</sub>-T<sub>0</sub> after 100 ns, which corresponds to dehybridization of 6–7 base pairs out of 30 (Figure 4, number of H-bond are listed under each image). While some of the initial base pairings broke apart in cage-T<sub>3</sub>-T<sub>3</sub>, the number of H-bonds was still 69 due to formation of additional non-Watson–Crick hydrogen bonds from non-complementary thymine spacers. The formation of these non-traditional H-bonds was more evident in cage-T<sub>6</sub>-T<sub>6</sub>, where the total number of H-bonds increased from 69 to 79. These results suggest that non-complementary thymine spacers can play important roles in the stabilization of the cage structures by minimizing the exposed hydrophobic surfaces of the cores. In the absence of such spacers, such as in the case of cage-T<sub>0</sub>-T<sub>0</sub>, the cage structure is so severely disturbed to compensate for the exposed hydrophobic organic cores that it cannot even form; instead, ill-defined networks are favored, as observed in our experiments.

We note that Sleiman and co-workers recently observed the *exclusive* formation of an insoluble ill-defined network when they combined two "fully complementary" rSMDH<sub>3</sub>'s, where the ss-DNA arms are directly attached to a tetraphenyl core without any spacer in between, at 3  $\mu\text{M}$  concentration.<sup>20</sup> The large size of these networks was confirmed by their zero electrophoretic mobility in PAGE-gel, and they can be visualized as infinite networks by AFM. These results are identical to what we observed for our cage-T<sub>0</sub>-T<sub>0</sub> dimer and reinforced our observations that ill-defined networks are greatly

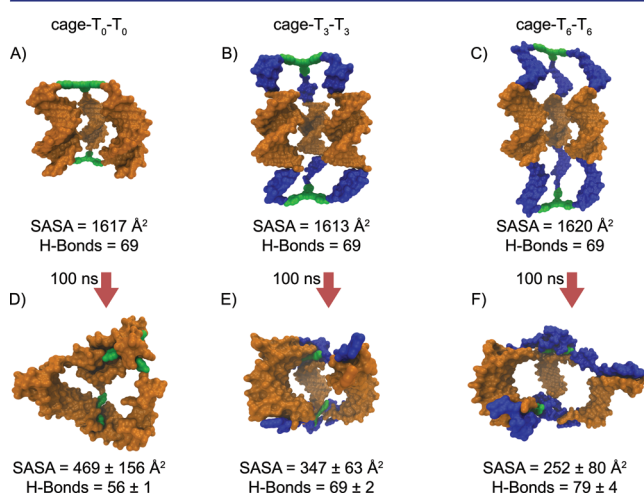


**Figure 4.** Molecular-surface representation of cage dimers before (A–C) and after (D–F) 100 ns MD simulations: cage-T<sub>0</sub>-T<sub>0</sub> (A, D), cage-T<sub>3</sub>-T<sub>3</sub> (B, E), and cage-T<sub>6</sub>-T<sub>6</sub> (C, F). Final structures are taken from MD simulations with lowest SASA values. Green, organic core; blue, non-complementary thymine spacers; orange, 10-bp complementary ss-DNA arms that can form ds-DNA duplexes. We note that although the final lowest-SASA structure of cage-T<sub>0</sub>-T<sub>0</sub> (D) has the organic cores wrapped within the DNA arms, the DNA duplexes are significantly distorted as evidenced by the large average root-mean-square deviation (rmsd) of DNAs from B-form conformation (5.8 Å, see also Table S7 in the Supporting Information).

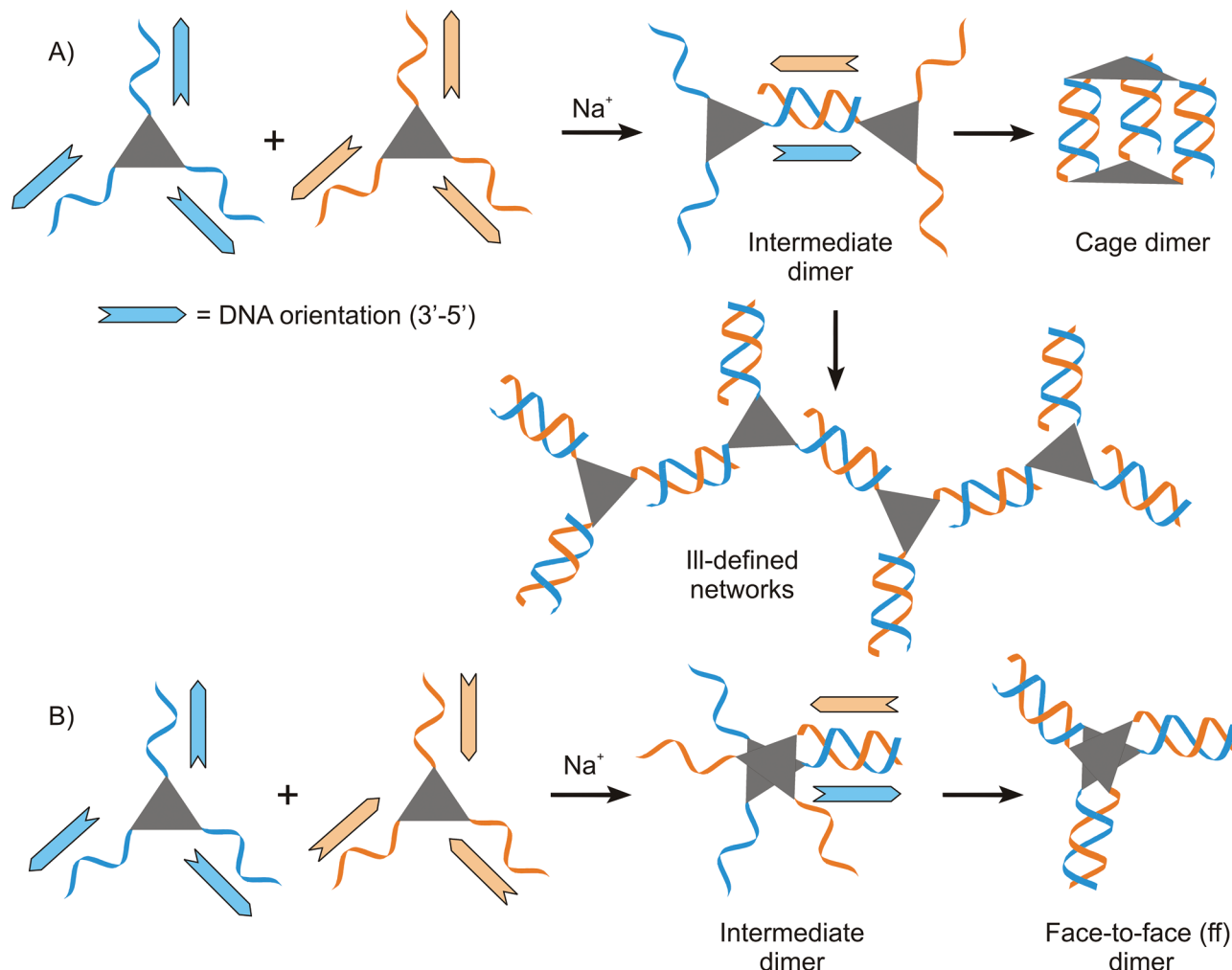


**Figure 5.** Schematic representation of cage (A) and face-to-face (B) dimers being formed from rSMDH<sub>3</sub> building blocks.

preferred over discrete [rSMDH<sub>3</sub>:rSMDH<sub>3</sub>] cages in the absence of non-complementary bases.

**New Design for Discrete Face-to-Face Dimers That Take Advantage of Hydrophobic Interactions.** Although hydrophobic interaction has not been previously identified as a major parameter that governed the assembly of rSMDH-based assemblies, it has been shown to be the primary interaction that induces the formation of supramolecular hairpin assemblies based on hydrophobic stacking of PDI cores.<sup>16,18</sup> With this in mind, we then set out to build a discrete [rSMDH<sub>3</sub>:rSMDH<sub>3</sub>] assembly that take advantage of *both* the hydrogen-bonding capability of the DNA-duplex arms and the hydrophobic interaction between the organic cores. Our experimental observations and MD simulations clearly demonstrated that the selectivity for cage vs ill-defined network formation is controlled not only by the concentration of the rSMDH<sub>3</sub> building blocks but also by how well the final assembled structure can minimize exposure of the hydrophobic surfaces of the organic cores. In the assembly of our cage dimer, after the first DNA arms are hybridized together from the two complementary rSMDH<sub>3</sub> building blocks, the two cores are spaced far apart from each other and thus have the potential to form linkages that “grow outward” to form a network at higher concentration (Figure 5A). If the DNA sequences and their orientations with respect to the core can be redesigned in such a way that the assembly process from the two complementary

rSMDH<sub>3</sub> building blocks would “push” the cores together after the first strands hybridize, the cores may be in close enough proximity for hydrophobic interaction and possible stacking (Figure 5B) that leads to *exclusive formation of a face-to-face dimer*. We predict that such an assembly would have enhanced melting temperature compared to simple DNA duplexes as well as comparable cage dimers because it can take advantage of both hydrophobic core-stacking and DNA hybridization.

**Molecular Dynamics Simulations of Face-to-Face Dimers.** To evaluate the stability of the aforementioned ff dimer structures, we carried out implicit solvent MD simulations on model systems representing ff-T<sub>0</sub>-T<sub>0</sub>, ff-T<sub>3</sub>-T<sub>0</sub>, and ff-T<sub>6</sub>-T<sub>0</sub> dimer structures using the same methodology as discussed above for the cage dimers. As before, initial structures of the ff dimers were constructed with three 10-bp ds-DNA arms attached to the organic cores, which were placed in the model as far away as possible from the DNA bases and base pairs (Figure 6A–C) at the beginning of the simulation. All final structures after MD simulations (100 ns) exhibited a planar arrangement of all the hybridized duplex arms (Figure 6D–F), with the cores in each structure either stacked directly on top of each other (Figure 7) or in close proximity at an average center-of-mass distance between 5 and 13 Å (Table S6 in the Supporting Information). These organic cores either intercalated into the base pairs (see Figure 6A for ff-T<sub>0</sub>-T<sub>0</sub>) or were wrapped by non-complementary thymine spacers (see

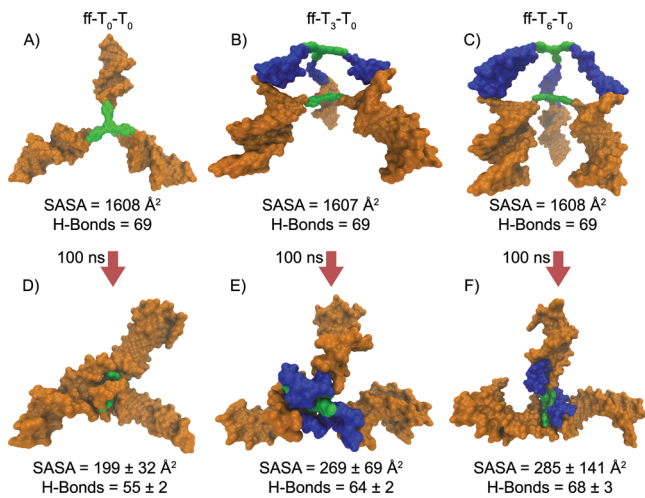


**Figure 6.** Molecular-surface representation of face-to-face dimers before (A–C) and after (D–F) 100 ns MD simulations: ff-T<sub>0</sub>-T<sub>0</sub> (A, D), ff-T<sub>3</sub>-T<sub>0</sub> (B, E), and ff-T<sub>6</sub>-T<sub>0</sub> (C, F). Final structures are taken from MD simulations with lowest SASA values. Side views are shown in B and C to emphasize the 3D structures. Top views of the structures are shown in A, D, E, and F. Green, organic core; blue, non-complementary thymine spacers; orange, 10-bp complementary ss-DNA arms that can form ds-DNA duplexes.

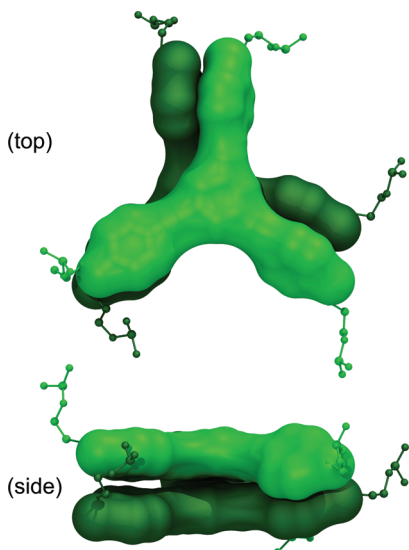


**Figure 7.** Top and side views of the hydrophobic cores being stacked on top of each other in the ff-T<sub>0</sub>-T<sub>0</sub> final structure. Light and dark green-colored molecular surfaces distinguish the individual cores.

Figures 6E for ff-T<sub>3</sub>-T<sub>0</sub> and ff-T<sub>6</sub>-T<sub>0</sub> and 6F) to minimize exposure of the hydrophobic surfaces of the cores to the aqueous solvent.

SASA analysis for all three ff dimers showed that they are all in the range of 199–285  $\text{\AA}^2$  (Figure 6, SASA values are listed under each image), which is lower than those found for the experimentally observed cage-T<sub>6</sub>-T<sub>6</sub> and cage-T<sub>3</sub>-T<sub>3</sub> dimers (252–347  $\text{\AA}^2$ , Figure 4, SASA values are listed under each image). These lower SASA values can be attributed to the hydrophobic interactions between the cores observed in the simulations, which help to minimize the exposure of the cores to the aqueous media without significantly disturbing the DNA duplexes, and suggests that the ff dimers would be stable and can be observed experimentally.

As in the case of the caged dimers, the total number of H-bonds within the hybridized DNA duplex arms in the ff dimers 69 at the start of the simulation. The final ff-T<sub>3</sub>-T<sub>0</sub> and ff-T<sub>6</sub>-T<sub>0</sub> structures did not deviate significantly from this number (64 and 68 H-bonds, respectively), suggesting that there is no significant rearrangement of the DNA arms to minimize exposure of the hydrophobic surfaces of the cores. Surprisingly, while the ff-T<sub>0</sub>-T<sub>0</sub> dimer has lost 14 H-bonds from the hybridized duplex arms, its SASA value remains much lower than that of the other two ff dimers, suggesting that this H-bond lost did not destabilize the structure at all, in stark contrast to that observed in the cage-T<sub>0</sub>-T<sub>0</sub> dimer (see Figure 4 and accompanying discussion above). This enhanced stability can be directly attributed to the unique face-to-face conformation of the two organic cores in ff-T<sub>0</sub>-T<sub>0</sub> dimer, which benefits not only from the hydrophobic stacking of the cores (Figure 7) but also from an effective lengthening of the duplex arms: the stacked core–core units essentially linked two 10-bp duplexes together to create an effectively longer DNA duplex system (Figure 6D). In comparison to the high SASA values for the ff-T<sub>3</sub>-T<sub>0</sub> and ff-T<sub>6</sub>-T<sub>0</sub> dimers, the lower SASA value for the ff-T<sub>0</sub>-T<sub>0</sub> structure suggests that the hydrophobic stacking of the cores (Figure 7) is the more important contributor to this stabilization. Indeed, while the core–core stacking still occurs for ff-T<sub>3</sub>-T<sub>0</sub> and ff-T<sub>6</sub>-T<sub>0</sub>, the non-complementary thymine spacers can better wrap around the stacked core–core unit to reduce the SASA as well as the hydrophobic stacking interactions between the cores (Figure 6E,F). Indeed, MD simulations indicated that the average center-of-mass core-to-core distance in four sets of each ff dimer (5, 11, and 13  $\text{\AA}$  for ff-T<sub>0</sub>-T<sub>0</sub>, ff-T<sub>3</sub>-T<sub>0</sub>, and ff-T<sub>6</sub>-T<sub>0</sub>, respectively, see also Table S7 in the Supporting Information) increases as the spacer length increases

**Self-Assembly of Face-to-Face Dimers.** We were pleasantly surprised to observe exclusive formation of stable ff dimer structures (Table 3) from combining rSMDH<sub>3</sub>-XT<sub>0</sub>-3'

**Table 3. Face-to-Face Dimers Based on rSMDH<sub>3</sub>'s**

entry	components <sup>a</sup>	short name
1	rSMDH <sub>3</sub> -XT <sub>0</sub> -5':rSMDH <sub>3</sub> -XT <sub>0</sub> -3'	ff-T <sub>0</sub> -T <sub>0</sub>
2	rSMDH <sub>3</sub> -XT <sub>3</sub> -5':rSMDH <sub>3</sub> -XT <sub>0</sub> -3'	ff-T <sub>3</sub> -T <sub>0</sub>
3	rSMDH <sub>3</sub> -XT <sub>6</sub> -5':rSMDH <sub>3</sub> -XT <sub>0</sub> -3'	ff-T <sub>6</sub> -T <sub>0</sub>

<sup>a</sup>Total DNA concentration of 1 and 2  $\mu\text{M}$ .

and its complementary rSMDH<sub>3</sub>-XT<sub>n</sub>-5' ( $n = 0, 3$ , and 6) at 2  $\mu\text{M}$  total ss-DNA concentration. The non-denaturing PAGE-gel for these ff dimers shows one single clean band for each of these dimers (Figure 8). As the MD simulation suggested, and as shown by the optical melting profiles of these ff dimers (Figure 9), the hydrophobic core–core stacking in these assemblies resulted in dramatic increases in their melting temperatures ( $T_m$ 's) compared to the control-rSMDH<sub>3</sub>-T<sub>3</sub> and cage-T<sub>3</sub>-T<sub>3</sub> dimer: ff-T<sub>0</sub>-T<sub>0</sub> exhibited a dramatic 18.4 °C increase in  $T_m$  over the control-rSMDH<sub>3</sub>-T<sub>3</sub> assembly and a 14 °C increase in  $T_m$  over that for cage-T<sub>3</sub>-T<sub>3</sub> dimer. The extra stability in ff-T<sub>0</sub>-T<sub>0</sub> can be explained by the interactions of the stacked cores with the closest base pairs of the DNA duplex arms, similar to that observed in short DNA duplexes possessing hydrophobic end-capping agents.<sup>52</sup>

As we introduced T<sub>3</sub> and T<sub>6</sub> spacers into the rSMDH<sub>3</sub>-XT<sub>n</sub>-5' partner and use these to form ff-T<sub>3</sub>-T<sub>0</sub> and ff-T<sub>6</sub>-T<sub>0</sub> dimers, the melting temperatures of these dimers successively



**Figure 8.** Non-denaturing PAGE-gel image (6%) of DNA hybrids (2  $\mu$ M). From left to right: lane 1 = ff-T<sub>0</sub>-T<sub>0</sub>, lane 2 = ff-T<sub>3</sub>-T<sub>0</sub>, lane 3 = ff-T<sub>6</sub>-T<sub>0</sub>.

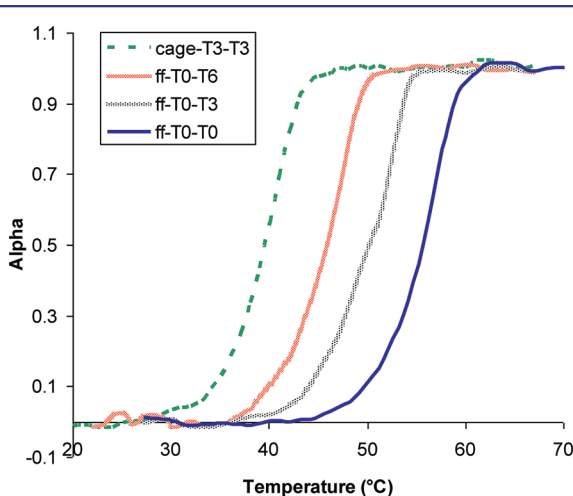


**Figure 9.** Melting profiles for ff-T<sub>n</sub>-T<sub>0</sub> ( $n = 0, 3$ , and  $6$ ) and cage-T<sub>3</sub>-T<sub>3</sub> (1  $\mu$ M) in PBS buffer (10 mM, pH 7.0, 75 mM NaCl).

decreased from that of the ff-T<sub>0</sub>-T<sub>0</sub> dimer, by 4 and 8  $^{\circ}$ C, respectively (Figure 9 and Table 4). Nevertheless, these are still significantly higher than those observed for the corresponding control-rSMDH<sub>3</sub>-T<sub>n</sub> assemblies and cage-T<sub>n</sub>-T<sub>n</sub> dimers ( $n = 0$ , 3, and 6; see Table 4). This trend confirms our observation in the MD simulations (see discussion above) that the T<sub>3</sub> and T<sub>6</sub> spacers can interact with the stacked core–core unit and decrease the hydrophobic stacking interactions that are primarily responsible for stabilizing the ff-T<sub>0</sub>-T<sub>0</sub> dimer (see C–C distance analysis in Table S7 in the Supporting Information).

Further evidence for the hydrophobic stacking of the cores in ff dimers is provided by the observation that the fluorescence of the core in rSMDH<sub>3</sub>-XT<sub>0</sub>-3' and its complementary rSMDH<sub>3</sub>-X'T<sub>0</sub>-5' partner is greatly quenched upon hybridization into the ff-T<sub>0</sub>-T<sub>0</sub> (Figure S34 in the Supporting Information) due to the increased interactions between the cores. This type of

**Table 4. Melting Data for cage-T<sub>n</sub>-T<sub>n</sub>, control-rSMDH<sub>3</sub>-T<sub>n</sub>, and ff-T<sub>n</sub>-T<sub>0</sub> ( $n = 0, 3$ , and  $6$ ) Assemblies with 1  $\mu$ M Total DNA Concentration in PBS Buffer (10 mM, pH 7.0, 75 mM NaCl)**

entry	short name	T <sub>m</sub> (°C)	fwlm (°C)
1	X:X'	36.6 $\pm$ 0.2	12.0 $\pm$ 0.1
2	control-rSMDH <sub>3</sub> -T <sub>0</sub>	39.2 $\pm$ 0.3	11.4 $\pm$ 0.1
3	control-rSMDH <sub>3</sub> -T <sub>3</sub>	36.5 $\pm$ 0.2	9.9 $\pm$ 0.1
4	control-rSMDH <sub>3</sub> -T <sub>6</sub>	37.4 $\pm$ 0.1	9.3 $\pm$ 0.1
5	"cage-T <sub>0</sub> -T <sub>0</sub> " <sup>a</sup>	41.2 $\pm$ 0.3	9.2 $\pm$ 0.1
6	cage-T <sub>3</sub> -T <sub>3</sub>	39.8 $\pm$ 0.3	7.0 $\pm$ 0.1
7	cage-T <sub>6</sub> -T <sub>6</sub>	39.6 $\pm$ 0.2	7.4 $\pm$ 0.1
8	cage-T <sub>3</sub> -T <sub>3</sub> -reverse	40.6 $\pm$ 0.1	7.3 $\pm$ 0.1
9	ff-T <sub>0</sub> -T <sub>0</sub>	55.6 $\pm$ 0.1	7.1 $\pm$ 0.1
10	ff-T <sub>3</sub> -T <sub>0</sub>	50.3 $\pm$ 0.3	7.2 $\pm$ 0.1
11	ff-T <sub>6</sub> -T <sub>0</sub>	46.0 $\pm$ 0.2	7.4 $\pm$ 0.1

<sup>a</sup>This structure did not form according to PAGE-gel study (see Figure 3).

quenching behavior has been observed in PDI-based hairpins as they formed supramolecular polymers based on stacking of PDI cores in high salt environment.<sup>18</sup> Indeed, the fluorescence of the three ff dimers (Figure 10) varies inversely with their

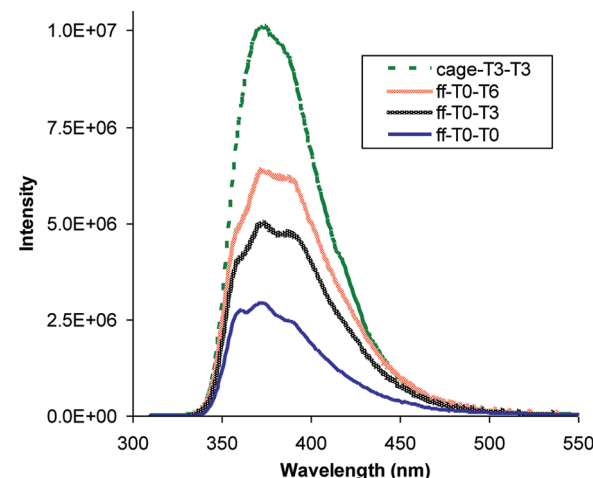


**Figure 10.** Fluorescent spectra of ff-T<sub>0</sub>-T<sub>0</sub> ( $n = 0, 3$ , and  $6$ ) and cage-T<sub>3</sub>-T<sub>3</sub> (1  $\mu$ M) dimers in PBS buffer (10 mM, pH 7.0, 75 mM NaCl); the excitation wavelength was 305 nm. The fluorescent spectrum of the cage-T<sub>3</sub>-T<sub>3</sub> assembly is provided as a reference point rather than that for the [rSMDH<sub>3</sub>-XT<sub>0</sub>-3':rSMDH<sub>3</sub>-X'T<sub>0</sub>-5'] assembly (Figure S34 in the Supporting Information) because quenching of the core by conformationally fixed DNA base pairs does occur to a certain extent.<sup>79</sup>

stability, which in turn is a function of the distance between the cores. Most interestingly, the fluorescence-based melting profile of ff-T<sub>0</sub>-T<sub>0</sub> closely mirrors its optical melting profile (Figure S37 in the Supporting Information), indicating that in the melting of the ff dimers, core–core unstacking occurs in a concerted manner as the dehybridization of the duplex arms.<sup>53,78</sup>

**Enhanced Melting Properties of Cage and Face-to-Face Dimers.** We have previously reported that cage dimers based on rSMDH<sub>2</sub><sup>23</sup> and rSMDH<sub>3</sub><sup>21</sup> building blocks can display cooperative melting behaviors (i.e., increased T<sub>m</sub> and sharpened melting profiles) in comparison to their free DNA analogues due to a combination of reduced configurational entropy and

ion-cloud sharing that occurs as a consequence of the proximity of their DNA duplex linkages. To these two parameters of the neighboring-duplex model<sup>28</sup> can now be added hydrophobic interactions, especially if the organic cores in rSMDH<sub>n</sub> are designed to be in the right orientation so that these interactions, and hydrophobic stacking, can play an important role, as in the case of ff-T<sub>0</sub>-T<sub>0</sub>. Indeed, the three ff-T<sub>n</sub>-T<sub>0</sub> ( $n = 0, 3$ , and  $6$ ) dimers reported herein all showed cooperative melting behaviors that are similar to those of the cage-T<sub>n</sub>-T<sub>n</sub> ( $n = 3$  and  $6$ ) dimers. The full-widths at half-max (fwhm's) of the derivative of the melting profiles for ff-T<sub>n</sub>-T<sub>0</sub> ( $n = 0, 3$ , and  $6$ ) and cage-T<sub>n</sub>-T<sub>n</sub> ( $n = 3$  and  $6$ ) dimers are all in the range of 7.0–7.4 °C, much sharper than those for the control-rSMDH<sub>3</sub>-T<sub>n</sub> systems (fwhm ~9.3–11.4 °C, see Table 4). This sharp melting behavior can be attributed to configurational entropy<sup>23,57</sup> and ion-cloud sharing between the DNA-duplex arms, all of which are in the 10–50 Å range required for ion-cloud sharing.<sup>80</sup>

The  $T_m$  of the ff-T<sub>0</sub>-T<sub>0</sub> dimer is dramatically higher compared to those for the control-rSMDH<sub>3</sub>-T<sub>0</sub> and cage-T<sub>3</sub>-T<sub>3</sub> dimer ( $\Delta T_m = 16.4$  and 15.8 °C, respectively, Table 4). However, as non-complementary T<sub>3</sub> and T<sub>6</sub> spacers were introduced into the ff dimers, the melting temperatures of ff-T<sub>3</sub>-T<sub>0</sub> and ff-T<sub>6</sub>-T<sub>0</sub> were decreased by 5.3 and 9.6 °C compared to that of the ff-T<sub>0</sub>-T<sub>0</sub> dimer. Yet, ff-T<sub>6</sub>-T<sub>0</sub> still melts at a higher temperature than the cage-T<sub>6</sub>-T<sub>6</sub> dimer ( $\Delta T_m = 6.4$  °C). These observations indicate that a large contribution to the extra thermal stability in the ff dimers stemmed from the core–core hydrophobic interactions that can be tuned by the length of the non-complementary thymine spacers. When there is no spacer, as in ff-T<sub>0</sub>-T<sub>0</sub>, this thermal stability can be further enhanced by the additional interaction of the stacked cores with the closest base-pairs from the DNA duplex arms, similar to that observed in duplexes with hydrophobic end-capping agents.<sup>52</sup> This was indeed observed in our MD simulations (Figure 6D).

## CONCLUSION

In summary, we have elucidated the important role that hydrophobic interactions play in the aqueous assembly of nanoscale organic-DNA hybrid cages and ff dimers from rSMDH<sub>n</sub> building blocks. These nanostructures are assembled in aqueous environments in such a way that minimizes the exposure of the hydrophobic surface of the organic cores, whether through hydrophobic interactions with the core in another rSMDH<sub>n</sub>, with the bases in the attached DNA strands, and/or with the base pairs in the final assembled structures. When exposure of the hydrophobic surfaces of the cores could not be properly minimized in a dimer conformation, an ill-defined network can result, as in the case of cage-T<sub>0</sub>-T<sub>0</sub> dimer made from rSMDH<sub>3</sub> building blocks. On the other hand, if a dimer can be formed with good minimization of the hydrophobic surfaces of the cores, highly stable structures with enhanced melting points and cooperative melting profiles can be obtained. When hydrophobic stacking between the cores is the dominant interaction, such as in the case of ff dimers, dramatic increases in the melting temperature can be obtained. In the world of nanoscale DNA-linked structures, these results place hydrophobic interactions at the same level of importance as the number of ss-DNA surrounding the organic core; the orientation, geometry, and concentration of the strands; and the type and concentration of the salts in the assembly media. We are confident that such interactions can be utilized effectively as a design parameter in future applications of DNA-linked materials.

## ASSOCIATED CONTENT

### Supporting Information

Synthesis of phosphoramidite core and rSMDHs; HPLC traces and MALDI-ToF spectra of rSMDHs; optical melting profiles, first derivatives of the melting profile, fwhm, and error analysis of all assemblies; fluorescent spectra of ff dimers and their rSMDH precursors; fluorescence-based melting profiles of ff-T<sub>0</sub>-T<sub>0</sub> dimer; and molecular dynamics simulations and analysis details. Complete refs 60, 61, 62, and 65. This material is available free of charge via the Internet at <http://pubs.acs.org>.

## AUTHOR INFORMATION

### Corresponding Author

schatz@chem.northwestern.edu; stn@northwestern.edu

### Notes

The authors declare no competing financial interest.

## ACKNOWLEDGMENTS

We thank Prof. Frederick D. Lewis for insightful discussions regarding the fluorescence self-quenching experiments. Dr. Ilyas Yildirim thanks the Faculty of Science, Akdeniz University (Antalya, Turkey) for providing him with a working environment during the preparation of this manuscript. Financial support for this work was provided by the Air Force Office of Scientific Research under agreement FA-9550-11-1-0275 and the NSF (Grant EEC-0647560 through the NSEC program).

## REFERENCES

- (1) Bloomfield, V. A.; Crothers, D. M.; Tinoco, I. *Nucleic Acids: Structures, Properties, and Functions*; University Science Books: Sausalito, CA, 2000.
- (2) Seeman, N. C. *Nature* **2003**, *421*, 427–431.
- (3) Lin, C.; Liu, Y.; Rinker, S.; Yan, H. *ChemPhysChem* **2006**, *7*, 1641–1647.
- (4) Lin, C.; Liu, Y.; Yan, H. *Biochemistry* **2009**, *48*, 1663–1674.
- (5) Rothemund, P. W. K. *Nature* **2006**, *440*, 297–302.
- (6) Zhang, C.; He, Y.; Su, M.; Ko, S. H.; Ye, T.; Leng, Y.; Sun, X.; Ribbe, A. E.; Jiang, W.; Mao, C. *Faraday Discuss.* **2009**, *143*, 221–233.
- (7) Lo, P. K.; Metera, K. L.; Sleiman, H. F. *Curr. Opin. Chem. Biol.* **2010**, *14*, 597–607.
- (8) He, Y.; Ye, T.; Su, M.; Zhang, C.; Ribbe, A. E.; Jiang, W.; Mao, C. *Nature* **2008**, *452*, 198–201.
- (9) Andersen, E. S.; Dong, M.; Nielsen, M. M.; Jahn, K.; Subramani, R.; Mamdouh, W.; Golas, M. M.; Sander, B.; Stark, H.; Oliveira, C. L. P.; Pedersen, J. S.; Birkedal, V.; Besenbacher, F.; Gothelf, K. V.; Kjems, J. *Nature* **2009**, *459*, 73–76.
- (10) Le, J. D.; Pinto, Y.; Seeman, N. C.; Musier-Forsyth, K.; Taton, T. A.; Kiehl, R. A. *Nano Lett.* **2004**, *4*, 2343–2347.
- (11) Zheng, J.; Constantinou, P. E.; Micheel, C.; Alivisatos, A. P.; Kiehl, R. A.; Seeman, N. C. *Nano Lett.* **2006**, *6*, 1502–1504.
- (12) Li, H.; Park, S. H.; Reif, J. H.; LaBean, T. H.; Yan, H. *J. Am. Chem. Soc.* **2003**, *126*, 418–419.
- (13) Yan, H.; Park, S. H.; Finkelstein, G.; Reif, J. H.; LaBean, T. H. *Science* **2003**, *301*, 1882–1884.
- (14) Liu, Y.; Lin, C.; Li, H.; Yan, H. *Angew. Chem., Int. Ed.* **2005**, *44*, 4333–4338.
- (15) Shi, J.; Bergstrom, D. E. *Angew. Chem., Int. Ed.* **1997**, *36*, 111–113.
- (16) Wang, W.; Wan, W.; Zhou, H.-H.; Niu, S.; Li, A. D. Q. *J. Am. Chem. Soc.* **2003**, *125*, 5248–5249.
- (17) Abdalla, M. A.; Bayer, J.; Rädler, J. O.; Müllen, K. *Angew. Chem., Int. Ed.* **2004**, *43*, 3967–3970.
- (18) Neelakandan, P. P.; Pan, Z.; Hariharan, M.; Zheng, Y.; Weissman, H.; Rybtchinski, B.; Lewis, F. D. *J. Am. Chem. Soc.* **2010**, *132*, 15808–15813.

- (19) Kuroda, T.; Sakurai, Y.; Suzuki, Y.; Nakamura, A. O.; Kuwahara, M.; Ozaki, H.; Sawai, H. *Chem.—Asian J.* **2006**, *1*, 575–580.
- (20) Aldaye, F. A.; Sleiman, H. F. *J. Am. Chem. Soc.* **2007**, *129*, 10070–10071.
- (21) Stepp, B. R.; Gibbs-Davis, J. M.; Koh, D. L. F.; Nguyen, S. T. J. *Am. Chem. Soc.* **2008**, *130*, 9628–9629.
- (22) Meng, M.; Ahlborn, C.; Bauer, M.; Plietzsch, O.; Soomro, S. A.; Singh, A.; Muller, T.; Wenzel, W.; Bräse, S.; Richert, C. *ChemBioChem* **2009**, *10*, 1335–1339.
- (23) Eryazici, I.; Prytkova, T. R.; Schatz, G. C.; Nguyen, S. T. J. *Am. Chem. Soc.* **2010**, *132*, 17068–17070.
- (24) Singh, A.; Tolev, M.; Meng, M.; Klenin, K.; Plietzsch, O.; Schilling, C. I.; Muller, T.; Nieger, M.; Bräse, S.; Wenzel, W.; Richert, C. *Angew. Chem., Int. Ed.* **2011**, *50*, 3227–3231.
- (25) Shchepinov, M. S.; Udalova, I. A.; Bridgman, A. J.; Southern, E. M. *Nucleic Acids Res.* **1997**, *25*, 4447–4454.
- (26) Scheffler, M.; Dorenbeck, A.; Jordan, S.; Wüstefeld, M.; von Kiedrowski, G. *Angew. Chem., Int. Ed.* **1999**, *38*, 3311–3315.
- (27) Shchepinov, M. S.; Mir, K. U.; Elder, J. K.; Frank-Kamenetskii, M. D.; Southern, E. M. *Nucleic Acids Res.* **1999**, *27*, 3035–3041.
- (28) Gibbs-Davis, J. M.; Schatz, G. C.; Nguyen, S. T. J. *Am. Chem. Soc.* **2007**, *129*, 15535–15540.
- (29) Alemdaroglu, F. E.; Ding, K.; Berger, R.; Herrmann, A. *Angew. Chem., Int. Ed.* **2006**, *45*, 4206–4210.
- (30) Ding, K.; Alemdaroglu, F. E.; Börsch, M.; Berger, R.; Herrmann, A. *Angew. Chem., Int. Ed.* **2007**, *46*, 1172–1175.
- (31) Waybright, S. M.; Singleton, C. P.; Tour, J. M.; Murphy, C. J.; Bunz, U. H. F. *Organometallics* **2000**, *19*, 368–370.
- (32) Waybright, S. M.; Singleton, C. P.; Wachter, K.; Murphy, C. J.; Bunz, U. H. F. *J. Am. Chem. Soc.* **2001**, *123*, 1828–1833.
- (33) Vargas-Baca, I.; Mitra, D.; Zulyniak, H. J.; Banerjee, J.; Sleiman, H. F. *Angew. Chem., Int. Ed.* **2001**, *40*, 4629–4632.
- (34) Stewart, K. M.; McLaughlin, L. W. *Chem. Commun.* **2003**, 2934–2935.
- (35) Mitra, D.; Di Cesare, N.; Sleiman, H. F. *Angew. Chem., Int. Ed.* **2004**, *43*, 5804–5808.
- (36) Stewart, K. M.; McLaughlin, L. W. *J. Am. Chem. Soc.* **2004**, *126*, 2050–2057.
- (37) Stewart, K. M.; Rojo, J.; McLaughlin, L. W. *Angew. Chem., Int. Ed.* **2004**, *43*, 5808–5811.
- (38) Mirkin, C. A.; Letsinger, R. L.; Mucic, R. C.; Storhoff, J. J. *Nature* **1996**, *382*, 607–609.
- (39) Alivisatos, A. P.; Johnsson, K. P.; Peng, X.; Wilson, T. E.; Loweth, C. J.; Bruchez, M. P.; Schultz, P. G. *Nature* **1996**, *382*, 609–611.
- (40) Elghanian, R.; Storhoff, J. J.; Mucic, R. C.; Letsinger, R. L.; Mirkin, C. A. *Science* **1997**, *277*, 1078–1081.
- (41) Taton, T. A.; Mirkin, C. A.; Letsinger, R. L. *Science* **2000**, *289*, 1757–1760.
- (42) Gibbs, J. M.; Park, S.-J.; Anderson, D. R.; Watson, K. J.; Mirkin, C. A.; Nguyen, S. T. J. *Am. Chem. Soc.* **2005**, *127*, 1170–1178.
- (43) Park, S. Y.; Lytton-Jean, A. K. R.; Lee, B.; Weigand, S.; Schatz, G. C.; Mirkin, C. A. *Nature* **2008**, *451*, 553–556.
- (44) Aldaye, F. A.; Sleiman, H. F. *Angew. Chem., Int. Ed.* **2006**, *45*, 2204–2209.
- (45) Aldaye, F. A.; Sleiman, H. F. *J. Am. Chem. Soc.* **2007**, *129*, 4130–4131.
- (46) Lo, P. K.; Karam, P.; Aldaye, F. A.; McLaughlin, C. K.; Hamblin, G. D.; Cosa, G.; Sleiman, H. F. *Nat. Chem.* **2010**, *2*, 319–328.
- (47) Macfarlane, R. J.; Lee, B.; Jones, M. R.; Harris, N.; Schatz, G. C.; Mirkin, C. A. *Science* **2011**, *334*, 204–208.
- (48) Yang, H.; Sleiman, H. F. *Angew. Chem., Int. Ed.* **2008**, *47*, 2443–2446.
- (49) Yang, H.; McLaughlin, C. K.; Aldaye, F. A.; Hamblin, G. D.; Rys, A. Z.; Rouiller, I.; Sleiman, H. F. *Nat. Chem.* **2009**, *1*, 390–396.
- (50) Dogan, Z.; Paulini, R.; Stütz, J. A. R.; Narayanan, S.; Richert, C. *J. Am. Chem. Soc.* **2004**, *126*, 4762–4763.
- (51) Patra, A.; Richert, C. *J. Am. Chem. Soc.* **2009**, *131*, 12671–12681.
- (52) Ng, P.-S.; Laing, B. M.; Balasundaram, G.; Pingle, M.; Friedman, A.; Bergstrom, D. E. *Bioconjugate Chem.* **2010**, *21*, 1545–1553.
- (53) Hariharan, M.; Zheng, Y.; Long, H.; Zeidan, T. A.; Schatz, G. C.; Vura-Weis, J.; Wasielewski, M. R.; Zuo, X.; Tiede, D. M.; Lewis, F. D. *J. Am. Chem. Soc.* **2009**, *131*, 5920–5929.
- (54) Andrews, A. T. *Electrophoresis: Theory, Techniques, and Biochemical and Clinical Applications*, 2nd ed.; Clarendon Press: Oxford, 1986.
- (55) Knotts, T. A.; Rathore, N.; Schwartz, D. C.; de Pablo, J. J. *J. Chem. Phys.* **2007**, *126*, 084901.
- (56) Drukker, K.; Schatz, G. C. *J. Phys. Chem. B* **2000**, *104*, 6108–6111.
- (57) Prytkova, T. R.; Eryazici, I.; Stepp, B.; Nguyen, S. B.; Schatz, G. C. *J. Phys. Chem. B* **2010**, *114*, 2627–34.
- (58) Sayar, M.; Avşaroğlu, B.; Kabakçioğlu, A. *Phys. Rev. E* **2010**, *81*, 041916.
- (59) Aldaye, F. A.; Sleiman, H. F. *Pure Appl. Chem.* **2009**, *81*, 2157–2181.
- (60) Case, D. A. et al. AMBER 9; University of California, San Francisco, 2006.
- (61) Case, D. A. et al. AMBER 10; University of California, San Francisco, 2006.
- (62) Case, D. A. et al. AMBER 11; University of California, San Francisco, 2006.
- (63) MacKerell, A. D., Jr.; Banavali, N.; Foloppe, N. *Biopolymers* **2000**, *56*, 257–265.
- (64) Hart, K.; Foloppe, N.; Baker, C. M.; Denning, E. J.; Nilsson, L.; MacKerell, A. D., Jr. *J. Chem. Theory Comput.* **2011**, *8*, 348–362.
- (65) Shaw, D. E.; et al. SIGARCH Comput. Archit. News **2007**, *35*, 1–12.
- (66) Klepeis, J. L.; Lindorff-Larsen, K.; Dror, R. O.; Shaw, D. E. *Curr. Opin. Struct. Biol.* **2009**, *19*, 120–127.
- (67) Wang, J.; Wolf, R. M.; Caldwell, J. W.; Kollman, P. A.; Case, D. A. *J. Comput. Chem.* **2004**, *25*, 1157–1174.
- (68) Cornell, W. D.; Cieplak, P.; Bayly, C. I.; Kollman, P. A. *J. Am. Chem. Soc.* **1993**, *115*, 9620–9631.
- (69) Cornell, W. D.; Cieplak, P.; Bayly, C. I.; Gould, I. R.; Merz, K. M.; Ferguson, D. M.; Spellmeyer, D. C.; Fox, T.; Caldwell, J. W.; Kollman, P. A. *J. Am. Chem. Soc.* **1995**, *117*, 5179–5197.
- (70) Bayly, C. I.; Cieplak, P.; Cornell, W.; Kollman, P. A. *J. Phys. Chem.* **1993**, *97*, 10269–10280.
- (71) Cieplak, P.; Cornell, W. D.; Bayly, C.; Kollman, P. A. *J. Comput. Chem.* **1995**, *16*, 1357–1377.
- (72) Wang, J.; Cieplak, P.; Kollman, P. A. *J. Comput. Chem.* **2000**, *21*, 1049–1074.
- (73) Yildirim, I.; Stern, H. A.; Kennedy, S. D.; Tubbs, J. D.; Turner, D. H. *J. Chem. Theory Comput.* **2010**, *6*, 1520–1531.
- (74) Pérez, A.; Marchán, I.; Svozil, D.; Sponer, J.; Cheatham, T. E., III; Laughton, C. A.; Orozco, M. *Biophys. J.* **2007**, *92*, 3817–3829.
- (75) Hawkins, G. D.; Cramer, C. J.; Truhlar, D. G. *J. Phys. Chem.* **1996**, *100*, 19824–19839.
- (76) Hawkins, G. D.; Cramer, C. J.; Truhlar, D. G. *Chem. Phys. Lett.* **1995**, *246*, 122–129.
- (77) Collaborative Computational Project, Number 4. *Acta Crystallogr., Sect. D* **1994**, *50*, 760–763.
- (78) Hariharan, M.; Siegmund, K.; Zheng, Y.; Long, H.; Schatz, G. C.; Lewis, F. D. *J. Phys. Chem. C* **2010**, *114*, 20466–20471.
- (79) Lewis, F. D.; Letsinger, R. L.; Wasielewski, M. R. *Acc. Chem. Res.* **2001**, *34*, 159–170.
- (80) Long, H.; Kudlay, A.; Schatz, G. C. *J. Phys. Chem. B* **2006**, *110*, 2918–2926.